Jurnal Ilmiah Teknik Elektro Komputer dan Informatika (JITEKI)
Vol. 9, No. 4, December 2023, pp. 1045-1059
ISSN: 2338-3070, DOI: 10.26555/jiteki.v9i4.26969

Intellectual System Diagnostics Glaucoma

Parul Ichhpujani[1], Vladimir Ryabtsev[2], Tetyana Utkina[3]
[1] Department of Ophthalmology, Government Medical College & Hospital, India
[2] Cherkassy Branch of the European University, Cherkassy, Ukraine
[3] Departments of Robotics and Specialized Computer Systems, Cherkasy State Technological University, Ukraine

ARTICLE INFO

Article history:

Received September 08, 2023
Revised October 30, 2023
Accepted November 10, 2023

Keywords :

Eyes;
Glaucoma;
Optic nerve;
Ophthalmology;
Optical coherence tomography

ABSTRACT

Glaucoma is a chronic eye disease that can lead to permanent vision loss. However, glaucoma is a difficult disease to diagnose because there is no pattern in the distribution of nerve fibers in the ocular fundus. Spectral analysis of the ocular fundus images was performed using the Eidos intelligent system. From the ACRIMA eye image database, 90.7% of healthy eye images were recognized with an average similarity score of 0.588 and 74.42% of glaucoma eye images with an average similarity score of 0.558. The reliability of eye image recognition can be achieved by increasing the number of digitized parameters of eye images obtained, for example, by optical coherence tomography. The research contribution is the digital processing of fundus graphic images by the intelligent system "Eidos". The scientific contribution lies in the automation of the glaucoma diagnosis process using digitized data. The results of the study can be used at medical faculties of universities to carry out automated diagnostics of glaucoma.

Corresponding Author:

Tatyana Utkina, Department of Robotics and Specialized Computer Systems,
Cherkassy State Technological University, 460 Shevchenko Boulevard, Cherkassy 18006, Ukraine.
Email: t.utkina@chdtu.edu.ua

1. INTRODUCTION

Glaucoma is an eye disease that, unlike cataracts, causes permanent and irreversible blindness. The exact pathophysiology of glaucoma is unknown, but basically the impaired aqueous outflow leads to increased intraocular pressure (IOP), which damages the optic nerve and causes vision and visual field loss. Due to population aging and increasing urbanization, in 2050, approximately 895 million people will have visual impairment, of which 61 million will be blind [1]. Artificial intelligence systems could revolutionize ophthalmology in the next decade by providing affordable, high-quality services in low- and middle-income countries. With age, intraocular pressure increases, causing disruption and loss of the retinal nerve fiber layer, so older patients are more likely to progress to glaucoma than younger patients [2]. To prevent insidious vision loss, regular eye examinations should be performed, with special attention paid to the condition of the retinal nerve fiber layer [3]. Men are more likely to have glaucoma than women also people of African descent are more likely to have glaucoma than people of European descent [4].

There are two main types of glaucoma: primary and secondary glaucoma, which have two main subtypes open-angle glaucoma and closed-angle glaucoma [5]. The co-modern treatment of glaucoma is aimed at reducing intraocular pressure with drugs, laser or surgery [6]. Macular vessel density and ganglion cell complex thickness of glaucoma-affected eyes are significantly lower than in healthy eyes, so measuring these parameters is useful for detecting glaucoma damage at an early stage [7]. Therefore, early diagnosis and treatment of glaucoma is crucial because in the early stages, glaucoma is not accompanied by symptoms such as pain or blurred vision, making it difficult to detect. Prevention of primary open-angle glaucoma requires availability of medications, regularity of administration, adherence to prescribed doses, and regular screening [8]. The state of the economies of countries determines health policies and affects the prevalence of glaucoma in the

population. Developing countries lack resources and personnel to provide ophthalmologic care, so glaucoma affects more population in such countries [9].

To classify healthy people and glaucoma patients, optical coherence tomography is used to measure the thickness of the nerve fiber layer of the retina. Using a retinograph camera, color photographs of the ocular fundus are obtained. The images of the eye fundus are recorded on the doctor's computer. Detailed examination allows to determine the part of dead nerve fibers that make up the nerve and to determine the degree of vision loss [10].

Clinical assessment of the optic nerve and IOP measurement are performed to detect glaucoma, but the use of these two parameters alone is not effective enough to diagnose all forms and stages of glaucoma. The most effective objective method is to document the parameters of the optic nerve of the eye during optical coherence tomography (OCT) or confocal scanning laser ophthalmoscopy (CSLO) using Heidelberg Retinal Tomograph (HRT) [11]. However, the sensitivity and accuracy of HRT is reduced in large eyes with myopic changes, and vascular pulsation can cause measurement bias.

Spectral domain optical coherence tomography imaging of the retina and optic disc is widely used to diagnose glaucoma and monitor disease progression [12]. SDOCT can be used to examine the elderly, people with high myopia, people with a family history of glaucoma, or people with elevated intraocular pressure [13]. SDOCT allows to establish the dependence of parameters of the optic nerve head and retinal nerve fiber layer depending on the stage of the disease [14]. Important parameters for image quality assessment are image resolution and depth [15]. Two main techniques are used in OCT: time domain OCT (TD-OCT) and spectral domain OCT (SD-OCT). SD-OCT allows the detection of individual retinal layers and lesion components [16]. OCT has been successfully used for ophthalmic visualization of the spectral region of the mouse retina [17]. The method of determining the density of peripapillary retinal vessels using the OCT system is promising [18].

In patients with glaucoma, the video ophthalmoscope registers a decrease in video signal amplitude in the microvascular tissue area of the optic disc [19]. Glaucoma is a multifactorial disease, the main risk factors are intraocular pressure, central corneal thickness, axis length, and ocular blood flow, but the relationship between risk factors and structural changes in the eye remains unclear [20]. OCT is used in ophthalmology as a painless, non-contact and non-invasive method of imaging areas of the retina, optic nerve and anterior segment of the eye. OCT allows obtaining high-quality images and distinguishing the structures of the eye down to micrometers (thousandths of a millimeter). Thus, OCT is both a scanner and a microscope, allowing a detailed view of the retinal structures. For scanning, OCT uses an infrared beam that passes through the structures of the eye, reaches the retina and, having been reflected, returns to the sensor, which records the returned signal [21]. A coilor image of the retina and nearby structures is formed on the basis of the data obtained.

An automated method of glaucoma screening by obtaining images of the ocular fundus using a smartphone connected to an optical lens to capture the retina is promising [22][23]. However, diagnosis of the disease from these images should be performed by an experienced ophthalmologist. Analysis of retinal fundus images is an attractive method for diagnosing glaucoma because the retina is the visible part of the nervous system, which is directly connected to the brain [24]. Color images of the ocular fundus contain 250000 or more pixels, so their processing is a rather time-consuming procedure that requires the use of automation tools. Methods such as median filtering, Gaussian filtering and wavelet transform are used to improve the quality of digital images and increase the accuracy of analysis by eliminating unwanted noise [25]. Due to the movement of the patient's eyes during OCT examination, special algorithms are required to ensure the accuracy of positioning [26]. Myopia is a risk factor for glaucoma development, but real structural changes in the eye make it difficult to recognize true glaucomatous changes [27]. During a comprehensive ophthalmologic examination, the thickness of the retinal nerve fiber layer is determined, which makes it possible to determine the glaucoma stage [28].

Deep Learning (DL) models based on convolutional neural networks (CNNs) can detect glaucoma by processing digital images of the retinal fundus. However, due to the insufficient number of recognized and labeled optic disc photographs, the diagnostic efficiency is limited, in addition, tools with high computational complexity are needed and special requirements are placed on the equipment used [29].

Glaucoma screening using artificial intelligence technology requires increased computational power and memory capacity for storing medical images [30]. Adding patient age and gender information improves the accuracy of glaucoma classification using deep learning system [31]. To reduce the computational complexity, images are downsampled using bilinear method. TIFF format is also used which preserves the original properties of the images without loss of information [32]. Publicly available datasets are used for training convolutional neural networks: ACRIMA, RIM-ONE, Harvard Dataverse (HVD) and Drishti, PAPILA [33].

Health care in underdeveloped countries faces significant challenges as annual inflation and demand for services grow faster than the ability to pay for care. At the same time, the use of mathematical models and large

databases has made it possible to personalize disease diagnosis and reduce the cost of health care down to the grassroots level.

2. RESEARCH METHOD

2.1. Formalization of the subject area

The ACRIMA database containing ocular fundus images of healthy and glaucoma-affected eyes collected at the FISABIO Oftalmología Médica Medical Center in Valencia, Spain, was used for the study [34]. The ACRIMA database was compiled by glaucoma specialists with many years of experience. The images are cropped around the optic disc and their descriptions do not include patient names. Examples of images of healthy eyes and eyes. Glaucoma affected eyes are shown in Fig. 1.

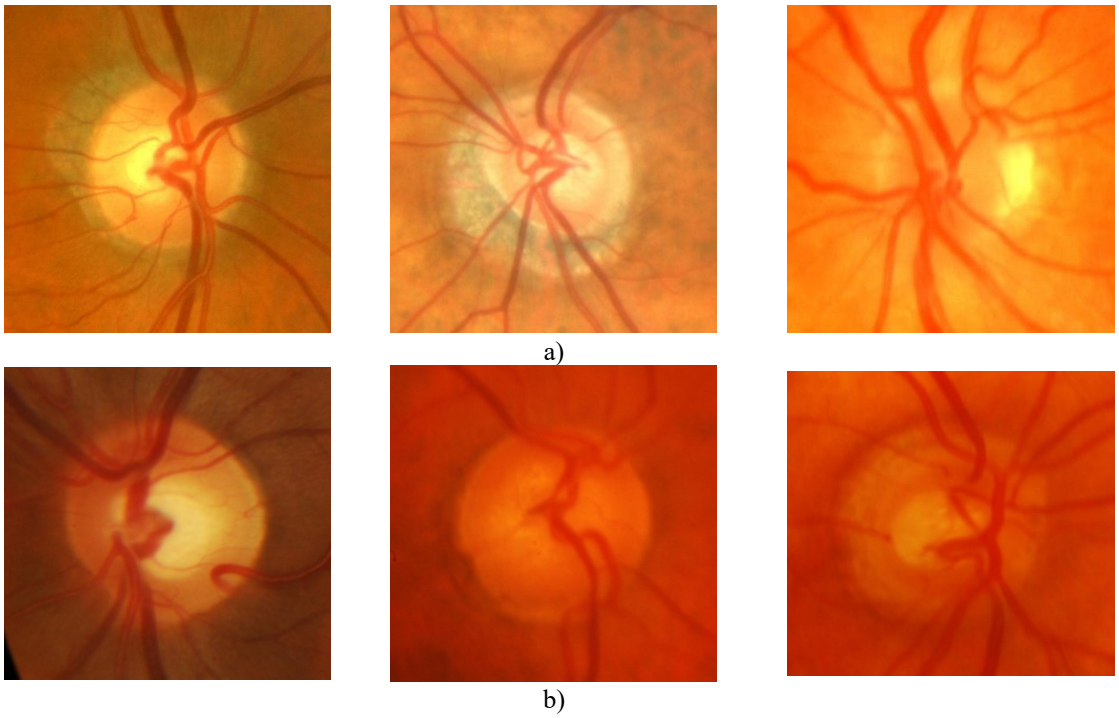

a)

b)

Fig. 1. Images of the optic nerves: a) Normal eyes; b) Eyes with glaucoma

Based on the quality of the neuroretinal sheath and peripapillary nerve fibers, an ophthalmologist can diagnose glaucoma, but with a large number of patients this is a tedious procedure and diagnostic errors are possible. Two directories Glaucoma_Negative and Glaucoma_Positive were created in the Inp_data folder on the Eidos disk, in which 43 images of healthy eyes and 43 images of eyes affected by glaucoma were placed. A fragment of the raw data is shown in Fig. 2. The number of images processed by the Eidos system is limited by the amount of memory it can process – 2 GB. For the selected number of ocular fundus images, the file size for storing images in internal format was 361 MB, and 1.8 GB was required to store the results of image pixel spectrum decomposition.

Inp_data

	A	B	C	D	E
1	SCALENAME	DATA_TYPE	OBJ1	OBJ2	OBJ3
2	Класс	C	Im001_ACRIMA	Im008_ACRIMA	Im016_ACRIMA
3	SPECTRINTERV: 1/21-{255,063,063}	N	0.0016	0.0012	0.0014
4	SPECTRINTERV: 2/21-{249,099,034}	N	18.3214	32.7314	12.8591
5	SPECTRINTERV: 3/21-{232,137,012}	N	0.0000	0.0000	0.0000
6	SPECTRINTERV: 4/21-{206,174,001}	N	0.8941	1.9727	5.4690
7	SPECTRINTERV: 5/21-{174,206,001}	N	0.0000	0.4280	2.4473
8	SPECTRINTERV: 6/21-{137,232,012}	N	0.0000	0.0000	0.0000
9	SPECTRINTERV: 7/21-{099,249,034}	N	0.0000	0.0000	0.0000
10	SPECTRINTERV: 8/21-{063,255,063}	N	0.0000	0.0000	0.0000

Fig. 2. Fragment of raw data for the study

Synthesis of image spectra was performed for 21 colors. The names of the images are given in the second row of the data, the remaining rows contain the components of the spectra. To form the model by the intelligent system "Eidos" the rows and columns of the data were rearranged as shown in Fig. 3. Class names were added to the second column.

Inp_data

	A	B	C	D
1	Image	Glaucoma	SPECTRINTERV: 1/21-{255,063,063}	SPECTRINTERV: 2/21-{249,099,034}
2	Im001_ACRIMA	Negative	0.0016	18.3214
3	Im008_ACRIMA	Negative	0.0012	32.7314
4	Im016_ACRIMA	Negative	0.0014	12.8591
5	Im017_ACRIMA	Negative	0.0014	14.0170
6	Im020_ACRIMA	Negative	0.0016	17.7263
7	Im025_ACRIMA	Negative	0.0019	16.4039
8	Im026_ACRIMA	Negative	0.0023	11.8629
9	Im030_ACRIMA	Negative	0.0018	31.9170
10	Im034_ACRIMA	Negative	0.0019	6.1857

Fig. 3. Input data format for the Eidos system

In this study, the method of digital processing of fundus graphic images was used. The software implementation of the method of image digitization was developed by D.K. Bandyk according to the algorithm and statement of Prof. E. V. Lutsenko [35]. The essence of the method of inputting images into the Eidos intellectual system is protected by a patent [36]. When performing automated system-cognitive (ASC) analysis of images by pixels, spectra and contours, the Eidos system measures the spectra of graphic objects, i.e. very precisely determines the colors present in the image. As an image spectrum, the system considers the proportion of pixels of different colors in the total number of pixels in the image. Several color ranges are used to measure image spectra. Each color range corresponds to a combination of brightnesses of red, green, blue rays, which in Eidos system by calculations form a spectrum. Generalized spectra of classes are formed in the Eidos system. Then specific objects are compared to classes by their spectra. Thus the total amount of information in colors of spectrum of concrete object about its belonging to the generalized image of class is calculated. Automation of the process of digitized data processing reduces the labor intensity and increases the reliability of glaucoma diagnosis.

The mode 2.3.2.5 of the intellectual system "Eidos" was used for image processing. The appearance of this mode of image processing is presented in Fig. 4.

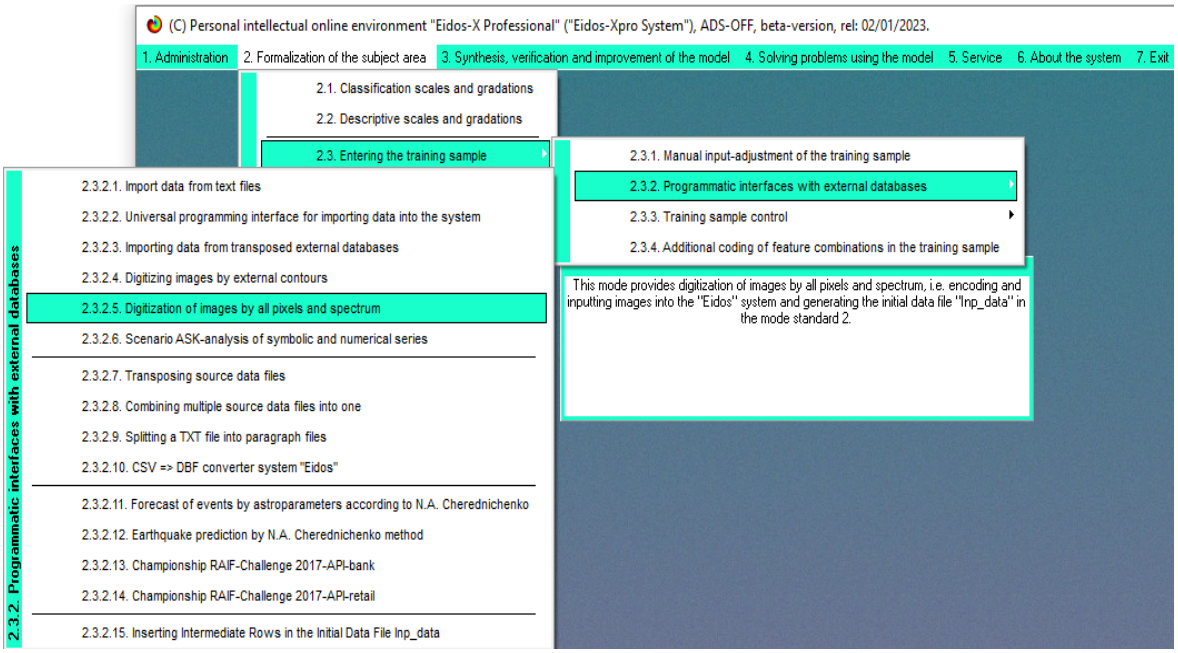

Fig. 4. Interface of image processing mode by pixels and spectrum

This mode provides conversion of images in bmp or jpg format into the source data file "lnp_data.xls", where each image is represented by a string. This source data file is used to formalize the subject area, create and verify models. The source images in the form of graphic files should be located in the folder: ...AID_DATA/INP_DATA/ and in subfolders. Names of folders and graphic files must meet the requirements of MS Windows. The duration of the image spectrum calculation for the selected number of images is very long and took 1.5 hours on a computer with an AMD Athlon 3.1 GHz processor with a 32-bit Windows 10 operating system.

2.2. Synthesis of cognitive models of the subject area

The formalizable cognitive concept was developed by Lutsenko E. V., which allows forming mathematical models of the studied subject area [37]. In the process of conducting experiments, connections between elements are revealed: some elements are observed frequently, while others rarely occur together. The presence of stable connections between elements suggests that they reflect some reality that is holistic with respect to these elements. This reality is called the "*objects of perception*". Considered in unity with the objects, the elements of perception are called "*signs of objects*". Thus, information about the features of objects observed in a particular subject area is formed.

Specific objects are given names and the objects are compared with each other. During the comparison, it is found that some objects are similar in their features, while others are different. Similar objects are grouped into generalized categories (classes) to which names are assigned. Classes are formalized using classification scales and gradations and represent an integral way of describing reality.

The principle of building mathematical models for ASC-analysis is based on system fuzzy interval mathematics. ASC-analysis was proposed by Prof. Lutsenko E. V. in 2002 in several articles and a fundamental monograph [38]. Currently, there are about 9 million sites with this word combination in the Internet on the corresponding query. It can be noted that specialists from several countries, including Canada, Russia, Belarus, and the USA, participated in the development of the Eidos system. Practical advice from Roger Donnay, a professional software developer, developer of the highly effective eXPress++ programming tool system, widely used in the creation of the Eidos system.

The essence of the mathematical model of ASC-analysis is as follows. A table of absolute frequencies is calculated directly from empirical data, after their formalization. In this table, rows correspond to the gradations of descriptive scales (values of factors), and columns – to classes, i.e. gradations of classification scales. At their intersection is the number of cases (facts) of observation of a certain value of a feature in objects of a certain class [39]. It is also a *fact* to observe the transition of the modeled object to some future state when it is affected by the value of some factor. It follows that in order to establish a fact, it is necessary to obtain a training sample containing features of objects, and on its basis create images of objects and identify each specific image, i.e. compare it with generalized images and determine the degree of their similarity. The Eidos system, like any other intellectual system, cannot initially do anything, it must first be trained. If there is no input data (training sample), it is impossible to conduct research in the Eidos system.

Seven specific INF1-INF7 knowledge criteria are used for model synthesis in ASC-analysis, and two integral similarity criteria, "Semantic Resonance of Knowledge" and "Sum of Knowledge", are used for model verification and solving the problem of identification and prediction [40]. The integral criterion "Sum of Knowledge" represents the total sum of knowledge contained in the system of factors of different nature, characterizing the control object, control factors and environment, regarding the transition of the object to future desirable or undesirable states. In coordinate form, this integral criterion is represented by the expression:

$$I_j = \sum_{i=1}^{M} I_{ij} I_i \tag{1}$$

where M – the number of descriptive scale gradations (features), I_j is the state vector of the j -th class, I_{ij} – state vector of the j -th class; L_i – is the state vector of the recognized object, which includes all types of factors characterizing the object itself, controlling influences, and the surrounding environment:

$$L_i \begin{cases} 1, if\ the\ i-th\ factor\ valid; \\ n, where\ n>0, if\ the\ i-th\ factor\ operates\ with\ truth\ n; \\ 0, if\ the\ i-th\ factor\ does\ not\ work. \end{cases}$$

Integral criterion "Semantic Resonance of Knowledge" is a normalized total sum of knowledge contained in the system of factors of different nature, characterizing the control object, control factors and environment,

regarding the transition of the object to future desirable or undesirable states. The integral criterion is an additive function of partial knowledge criteria and has the following form:

$$I_j = \frac{1}{\sigma_I \sigma_L M} \sum_{i=1}^{M} (I_{ij} - \bar{I}_j)(L_i - \bar{L}) \quad (2)$$

where M is the number of levels on the descriptive scale (features), $\bar{I}_j$ is the mean informativeness of the class vector, $\bar{L}$ is the mean of the object vector, σ_I is the standard deviation of the partial criteria of class vector knowledge; σ_L – is the standard deviation of the object vector recognition; $\overrightarrow{I_{ij}} = \{I_{ij}\}$ – the state vector of the j -th class; $\overrightarrow{L_i} = \{L_i\}$ – the state vector of the recognized object, which includes all types of factors that characterize the object itself, control actions and the environment (locator array), i.e.:

$$\overrightarrow{L_i} \begin{cases} 1, if\ the\ i-th\ factor\ valid; \\ n, where\ n > 0, if\ the\ i-th\ factor\ operates\ with\ truth\ n; \\ 0, if\ the\ i-th\ factor\ does\ not\ work. \end{cases}$$

In the Eidos system, the reliability of identification of the "k -th" grade of the class S_k is determined by the formula:

$$S_k = \frac{1}{N} \sum_{i=1}^{N} (BT_{ik} + T_{ik} - BF_{ik} - F_{ik}) \cdot 100\%, \quad (3)$$

where N – is the number of objects in the recognized sample; BT_{ik} – is the similarity level of the "i -th" object to the "k -th" grade to which it was correctly assigned by the system; T_{ik} – is the similarity level of the "i -th" object to the "k -th" grade to which it was correctly not assigned by the system; BF_{ik} – is the similarity level of the "i -th" object to the "k -th" grade to which it was erroneously assigned by the system; F_{ik} – is the similarity level of the "i -th" object to the "k -th" grade to which it was erroneously not assigned by the system. With such a definition, the similarity parameter varies from -100% to 100%.

The Eidos system provides simultaneous work with three statistical models and seven knowledge models, allowing to solve the problems of identification, decision-making and research of the subject area in all these models with the help of two integral criteria. The Eidos system evaluates the effectiveness of applying various partial and integral criteria to solve these problems.

2.3. Problem Formulation

In any training sample there is always present not only true information about the modeled subject area, but also some element of misinformation and noise. Noise and misinformation in the input data lead to a decrease in the validity of the models created on their basis. Artifacts called *"objects of the training sample"* whose features are random, or classes are random, or the relationship between the features of these objects and the belonging of these objects to classes is also random [41]. On the other hand, "*atypical objects of the training sample*" are those in which features and classes are not random, and the relationship between features and class membership of these objects, set in the training sample, is also not random, but quite regular. However, in the training sample the belonging of objects to classes can be set incorrectly. Therefore, it is necessary to have software tools to detect and suppress noise in the original data, as well as to detect misinformation in the original data and restore the true information. The Eidos system provides the mode of artifact detection, removal and typing. If according to the recognition results the level of similarity of the training sample object with the class is less than the specified threshold, this object is considered atypical (artifact). The threshold similarity level is specified as a percentage. You can remove atypical objects from the training sample or create new classes from atypical objects. These procedures can be repeated many times until new artifacts appear.

After removing artifacts whose object recognition accuracy is less than 25%, the model adequacy degrees shown in Fig. 5, and the L1-mean for the INF3 model became equal to 1,000. A total of 39 healthy eyes and 32 eyes with glaucoma remained in the training sample.

For each study, the Eidos system automatically generates 10 mathematical models and evaluates their validity according to several criteria: Van Risbergen's F-means and L1-means of Lutsenko. From Fig. 5 we can see that the L1-means for all ten models are different, so the most reliable model INF3 was chosen for the study. As can be seen from Fig. 5, the created semantic information model INF3 has a sufficiently high degree of reliability, i.e., it reflects the subject area under study quite adequately. The block diagram of the study using the Eidos system is shown in Fig. 6.

3.4. Generalized form for valid models at different int.crit. Current Model: "INF3"

Model name and private criterion	Integral criterion	S-precision models	S-Completeness models	L1-measure prof. E.V.Lutsenko
1. ABS - a particular criterion: the number of occurrences of combinati...	Correlation of abs.frequencies wit...	0.794	1.000	0.885
1. ABS - a particular criterion: the number of occurrences of combinati...	The sum of the absolute frequen...	0.810	1.000	0.895
2. PRC1 - particular criterion: arb. probability of the i-th feature among t...	Correlation of conditional relative ...	0.794	1.000	0.885
2. PRC1 - particular criterion: arb. probability of the i-th feature among t...	The sum of the conditional relativ...	0.792	1.000	0.884
3. PRC2 - particular criterion: conditional probability of the i-th feature i...	Correlation of conditional relative ...	0.794	1.000	0.885
3. PRC2 - particular criterion: conditional probability of the i-th feature i...	The sum of the conditional relativ...	0.792	1.000	0.884
4. INF1 - particular criterion: the amount of knowledge according to A. ...	Semantic resonance of knowledge	1.000	0.063	0.119
4. INF1 - particular criterion: the amount of knowledge according to A. ...	Sum of knowledge	0.996	1.000	0.998
5. INF2 - particular criterion: the amount of knowledge according to A. ...	Semantic resonance of knowledge	1.000	0.063	0.119
5. INF2 - particular criterion: the amount of knowledge according to A. ...	Sum of knowledge	0.996	1.000	0.998
6. INF3 - partial criterion: Xi-square, differences between actual and ex...	Semantic resonance of knowledge	1.000	1.000	1.000
6. INF3 - partial criterion: Xi-square, differences between actual and ex...	Sum of knowledge	1.000	1.000	1.000
7. INF4 - particular criterion: ROI (Return On Investment); probabilities f...	Semantic resonance of knowledge	1.000	0.062	0.117
7. INF4 - particular criterion: ROI (Return On Investment); probabilities f...	Sum of knowledge	0.994	1.000	0.997
8. INF5 - particular criterion: ROI (Return On Investment); probabilities f...	Semantic resonance of knowledge	1.000	0.062	0.117
8. INF5 - particular criterion: ROI (Return On Investment); probabilities f...	Sum of knowledge	0.994	1.000	0.997
9. INF6 - particular criterion: difference of conditional and unconditiona...	Semantic resonance of knowledge	1.000	1.000	1.000
9. INF6 - particular criterion: difference of conditional and unconditiona...	Sum of knowledge	0.991	1.000	0.996
10.INF7 - particular criterion: difference of conditional and uncondition...	Semantic resonance of knowledge	1.000	1.000	1.000
10.INF7 - particular criterion: difference of conditional and uncondition...	Sum of knowledge	0.991	1.000	0.996

Fig. 5. Generalized form of estimation of model reliability

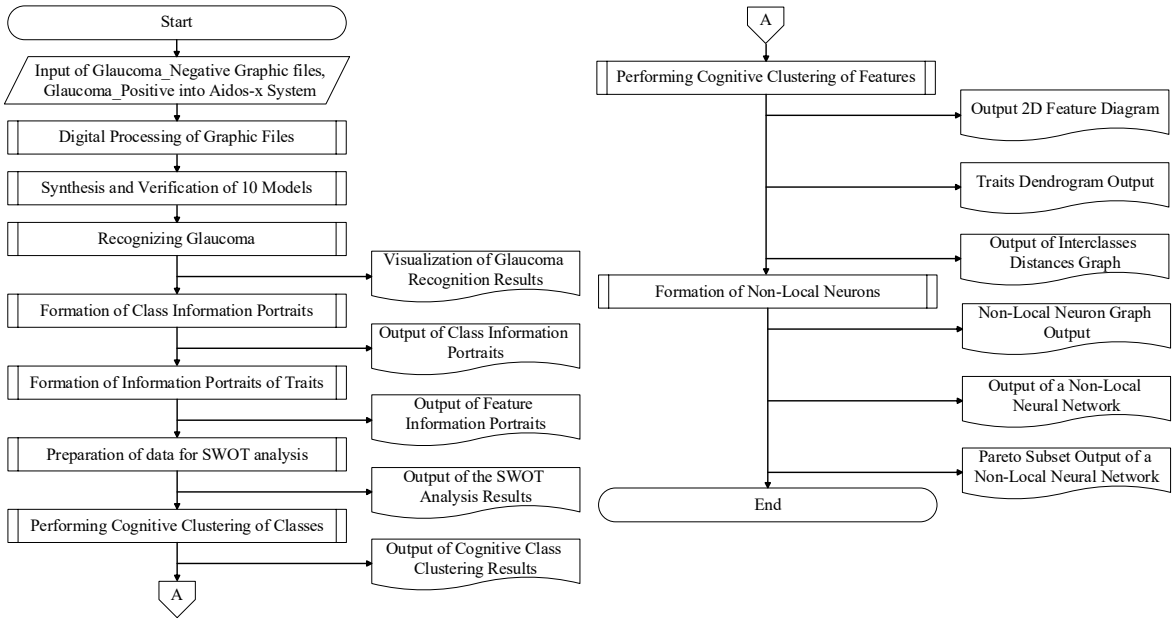

Fig. 6. Flowchart of the study execution

3. RESULTS AND DISCUSSION

Using the INF3 model with a high similarity value, images of healthy eyes (Fig. 7(a)) and eyes affected by glaucoma (Fig. 7(b)) were recognized.

The variability of the degree of similarity of samples with the class “Negative” ranges from 30.42 to 68.88. The variability of the degree of similarity of samples with the class “Positive” is from 38.00 to 100.00. To visually test the reliability of eye image recognition, the recognized images of healthy eyes and eyes with glaucoma were viewed by a glaucoma specialist [42]. It is not difficult for an experienced ophthalmologist to make a conclusion about the correctness of glaucoma recognition.

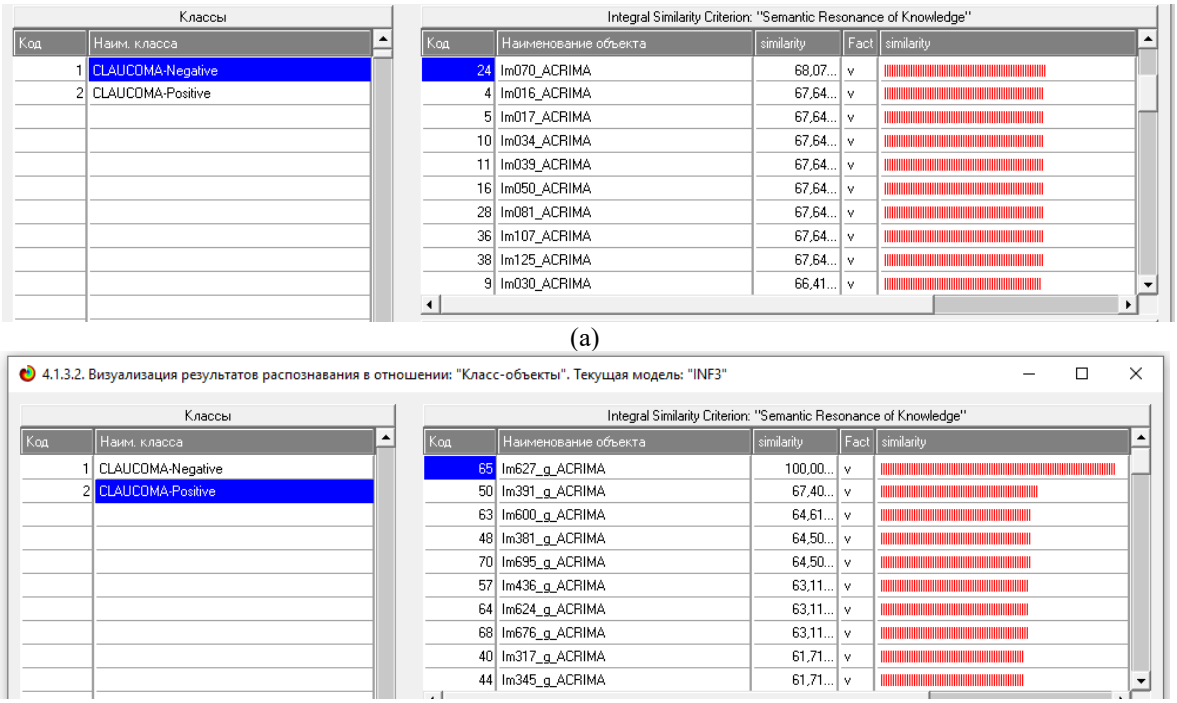

Fig. 7. Image recognition results: (a) Healthy eyes; (b) Eye with glaucoma

To increase the reliability of diagnosis, convolutional neural networks are trained on several hundreds of images, each of which contains several thousand pixels, so this procedure is very labor-intensive and time-consuming. In the proposed method, Eidos intelligent system is trained on digitized data. The number of eye fundus images is less than the training set of photographs required for convolutional neural networks. The digitization of the training sample eye photographs is done once by the Eidos intelligent system. After training, the graphical training photos can be deleted. To determine if a patient has glaucoma, only the fundus image is converted to a digital code, reducing the time required to prepare the raw data for the Eidos Intelligent System study.

The information portrait of the eye image area parameter is a list of classes ranked in descending order of the strength of influence of this parameter on the transition of the control object to the states corresponding to these classes. The first in this list are the states of the control object, on the transition to which this parameter has the greatest influence. Then the states on which this parameter has no significant influence are listed, and then the states – transitions to which this parameter prevents are listed. The information portrait of the SPECTRINTERY:7 parameter is shown in Fig. 8. The SPECTRINTERY:7 parameter has a positive influence on GLAUCOMA-Positive, the strength of influence is 0.500, and with the same strength this parameter has a negative influence on GLAUCOMA-Nedative. In further operations of the study, the names of the parameters are simplified and represented by the symbol “N” and the number of the color range.

The information portrait of the pattern recognition class showed the information contribution of each feature to the total amount of information contained in the generalized image of this class. The information portrait of a class is a list of factors ranked in descending order of their influence on the transition of the control object to the state corresponding to this class. The class information portraits presented in Fig. 9 show the equal importance of the digitized parameters for recognizing the eye image.

Class information portrait is a set of data and characteristics collected and analyzed by the Eidos intelligent system. Such a portrait contains information about the strength and direction of influence of features on the diagnosis of glaucoma. The researcher should carefully select those traits that have the greatest influence on the class condition. In general, the class information portrait can help the researcher to select the most important features and reduce the complexity of the study.

Quantitative SWOT-analysis of a class provides the construction of a SWOT-matrix for this class, indicating the strength of influence of facilitating and hindering factors directly on the basis of the training sample and, thus, is a tool for automated quantitative SWOT-analysis. The SWOT diagrams shown in Fig. 10 display the 14 most significant relationships, with the sign of the relationship displayed in color (red – plus, blue – minus) and the value reflected by the thickness of the line. It is possible to display diagrams only with positive or only with negative links.

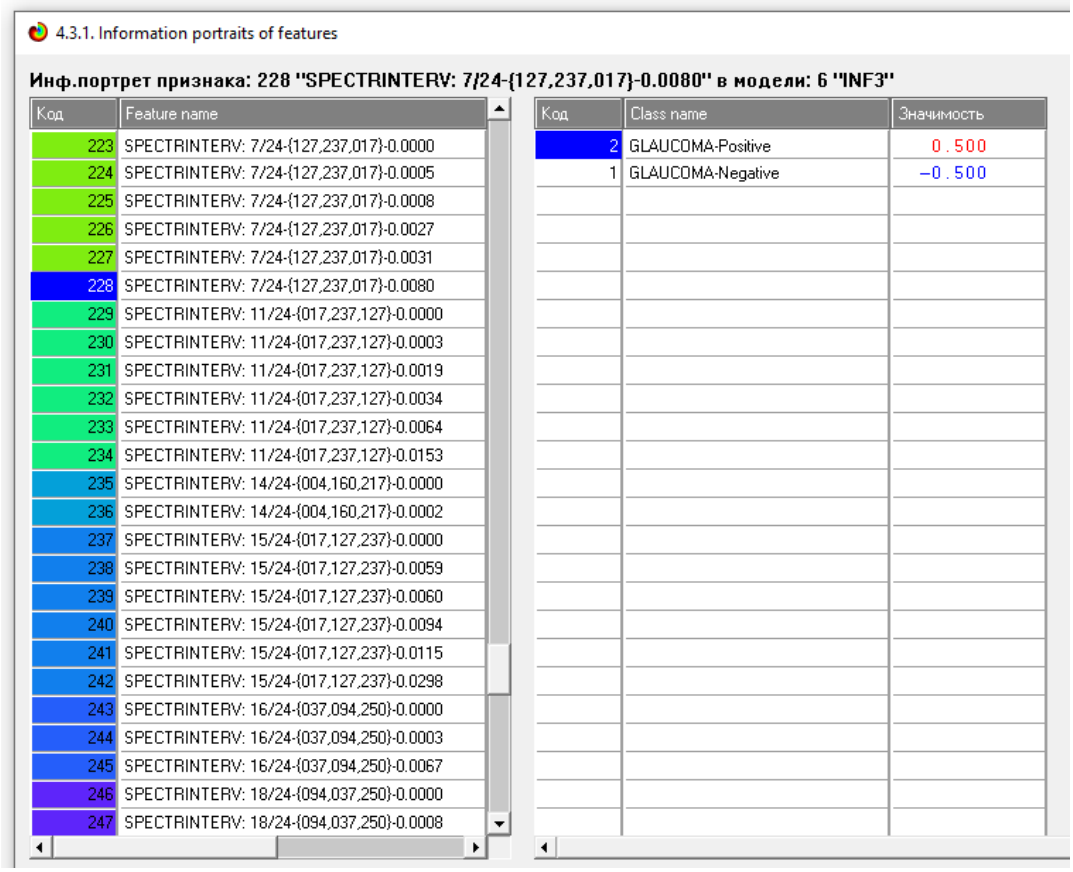

Fig. 8. Information portrait of parameter SPECTRINTERY:7

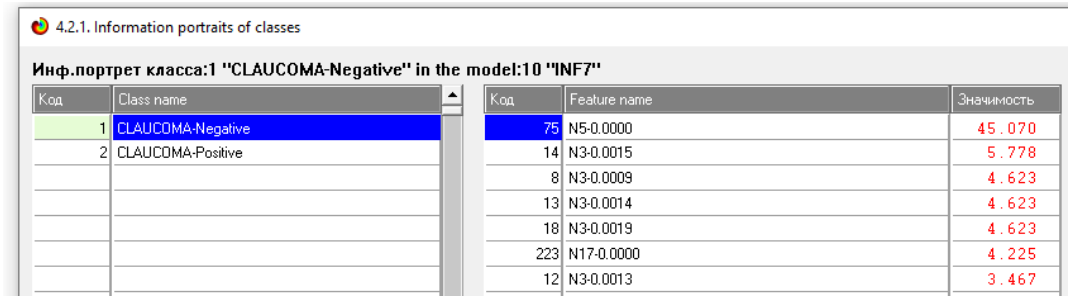

a)

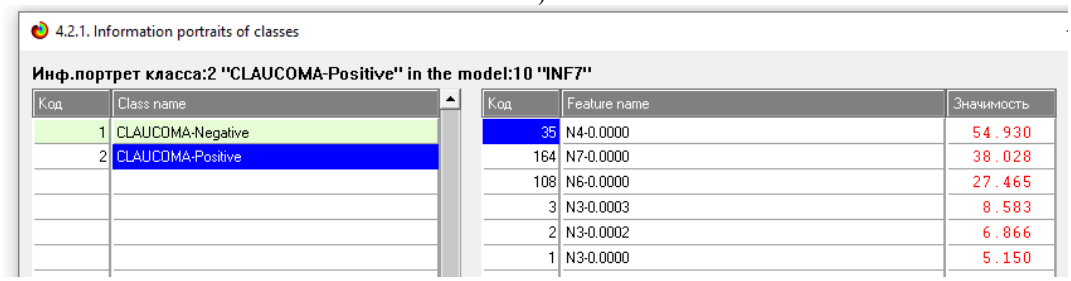

b)

Fig. 9. Information portraits of classes: (a) Negative; (b) Positive

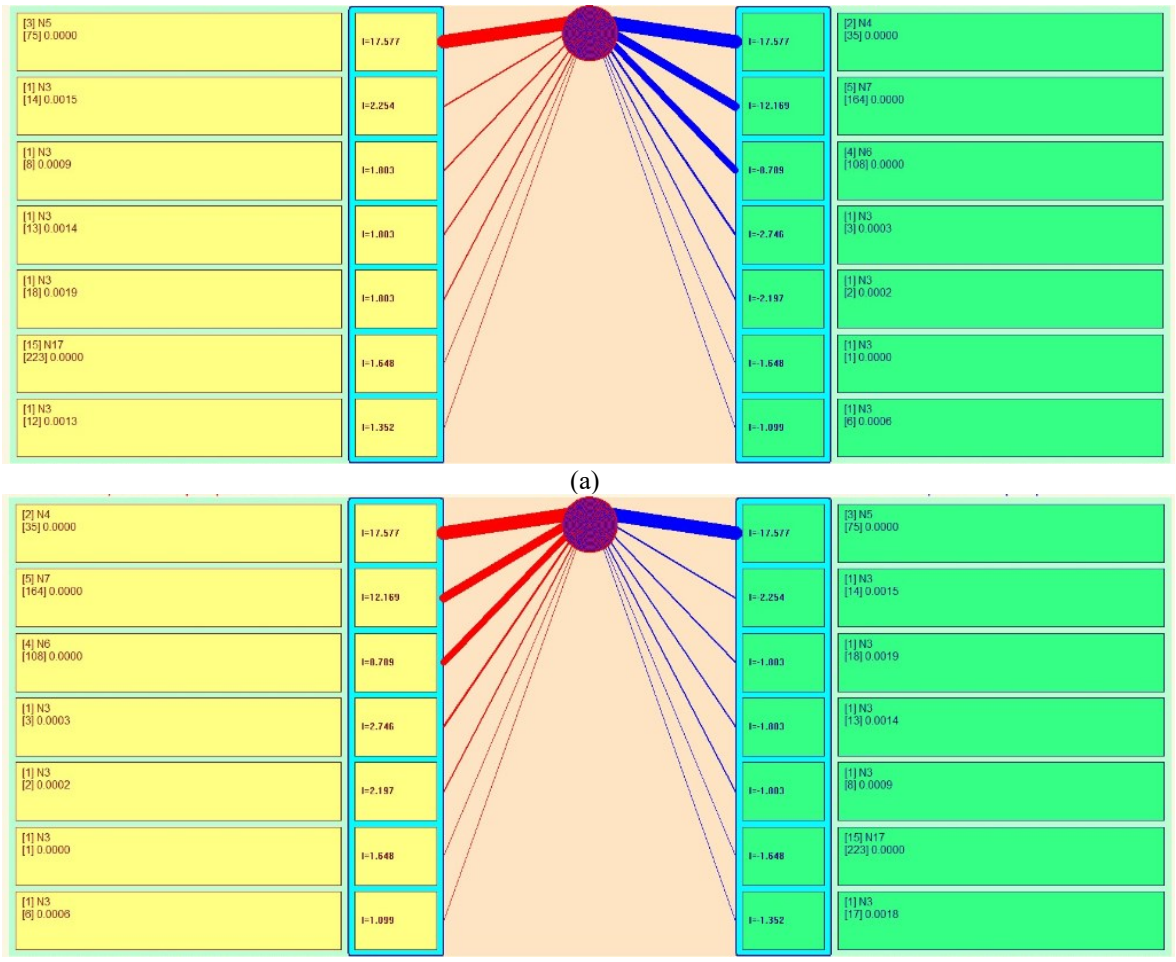

Fig. 10. Results of the SWOT-analysis of the classes: (a) Negative; (b) Positive

Non-local neurons in the Eidos system are visualized in the form of special graphical forms, on which the strength and direction of influence of neuron receptors on the degree of its activation/inhibition are displayed by the color and thickness of the dendrite. Non-local neurons are shown in Fig. 11. For clarity, only 20 neurons are shown, although there are 759 neurons in total. In the neural network layer image, the neurons are arranged in a circle. Neurons that positively affect the class score are shown in red, and neurons with a negative receptor value are shown in blue.

In the Eidos system it is possible to build models corresponding to multilayer neural networks. It is also possible to visualize any separate layer of a non-local neural network. Such a layer visually reflects the strength and direction of influence of receptors of several neurons on the degree of their activation/inhibition in the form of color and thickness of dendrites.

Fig. 12 shows the Pareto subset of the nonlocal neural network in the INF3 model containing 2 neurons for detecting eye damage in glaucoma. Activating synopses are shown in red and inhibiting synopses are shown in blue. Synopsis weights are indicated by circles. Digitized eye image parameters are used as receptors. Only 40.54% of the most significant synaptic connections are shown. If all connections were shown, this would be incomprehensible, but it emphasizes the complexity of the problem that needs to be addressed for proper diagnosis of glaucoma.

Fig. 13 shows the Pareto curve for the significance of descriptive scales (attributes). Almost one-third (17%) of the most significant attributes provide 50% of the overall significance. Half (50%) of the most significant attributes provide 72% of the total significance. The graph increases monotonically without a saturation region, which emphasizes the state when there are no redundant attributes in the task.

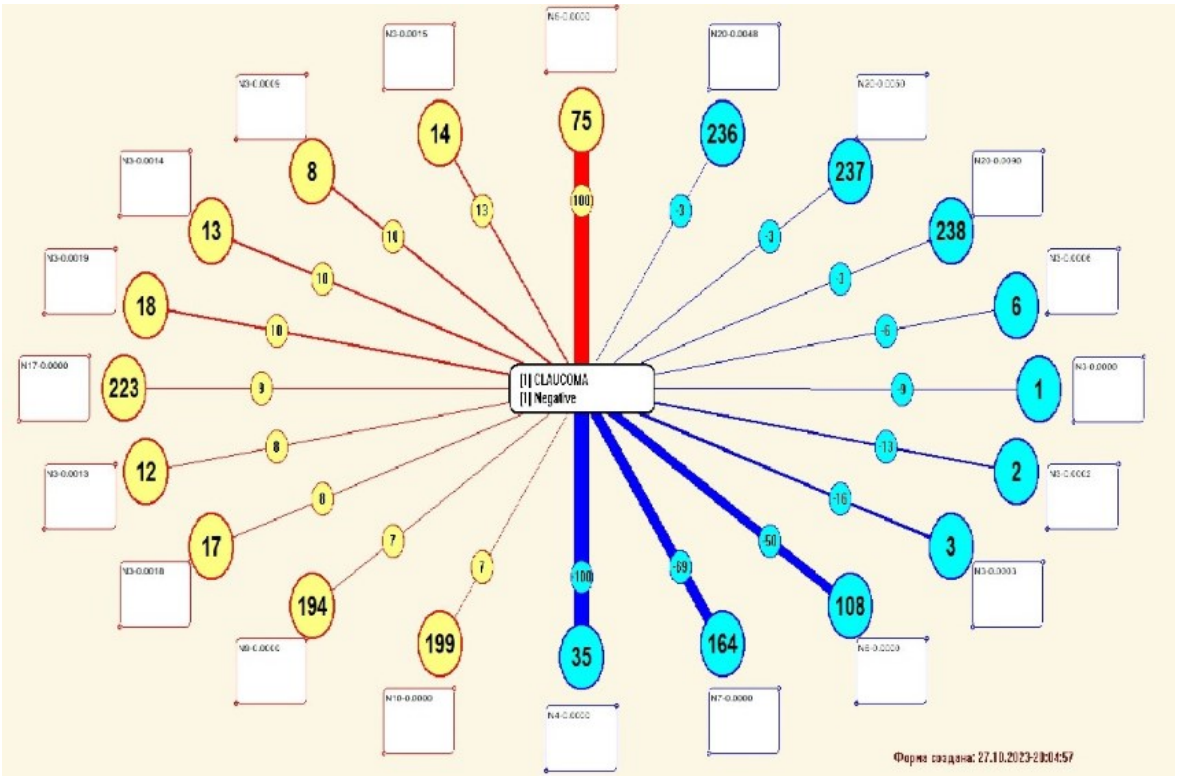

(a)

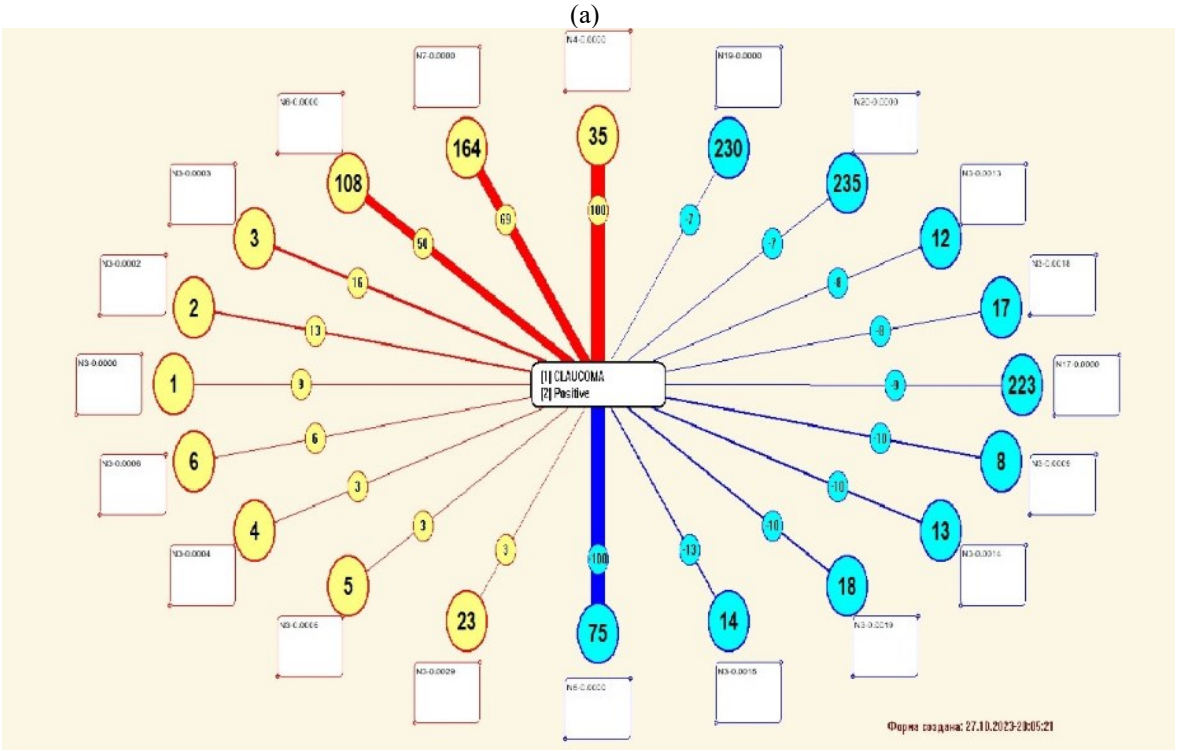

(b)

Fig. 11. Non-local class neurons: (a) Negative; (b) Positive

The procedure of Pareto curve construction allows selecting less significant features from the input data set and removing them, which reduces the complexity of its preparation. In the method of glaucoma diagnosis using convolutional neural networks there is no possibility to reduce the volume of input data.

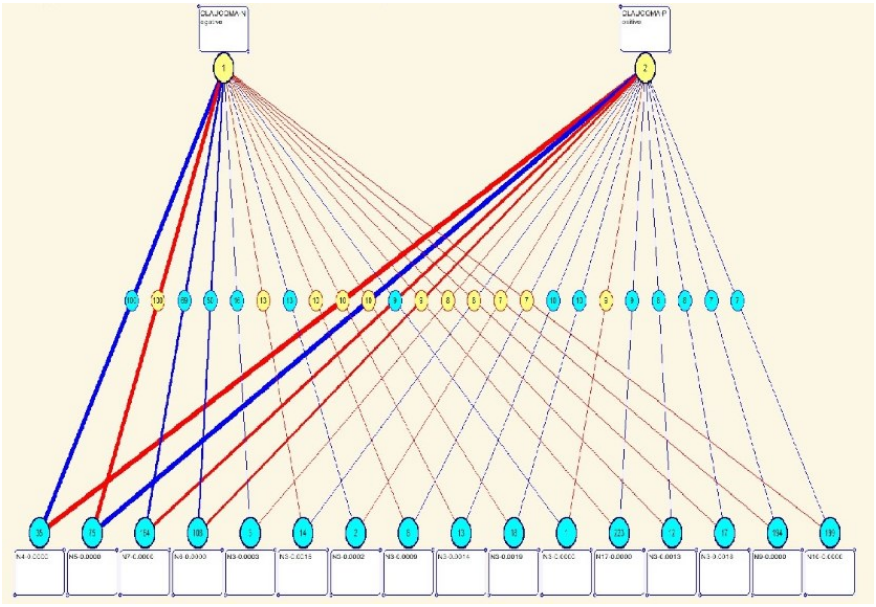

Fig. 12. Pareto subset of a non-local neural network

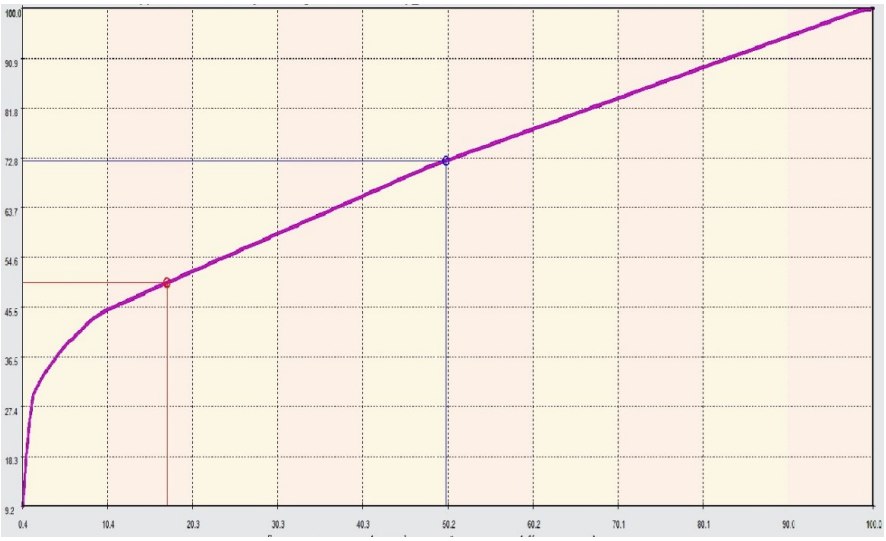

Fig. 13. Pareto curve for the significance of descriptive scales

Limitations

To load the transformed source data into the "Eidos" system, it is necessary to use the universal programming interface and specify the features of the data format. The data should be presented in Excel format. The spring 2011 version of the "Eidos" system provided for a training sample size of no more than 100,000 objects; in the current version this limitation has been removed, and now the system can work with millions of objects. However, there is still a limitation on the size of knowledge bases: no more than 4000 classes and 4000 gradations of factors. The universal intellectual system "Eidos" has a very complex user interface and 55 operating modes, not counting the "Exit" mode. It is almost impossible to learn how to work in this system on your own. Any mistake will lead to the system stopping or obtaining incorrect results [43]. If you start studying several modes of the system a day without any explanations, you will have to spend several months to learn how to work in the Eidos system. To reduce the training time, it is recommended to familiarize with the presentations posted at https://www.patreon.com/user? $u = 87599532$, which reveal the principles of using automated system-cognitive analysis to solve problem tasks.

4. CONCLUSION

ASC-image analysis provides automatic identification of image features by pixel colors, synthesis of generalized images (classes) of images, selection of the most characteristic features of images to distinguish

them, as well as solving problems of research of the simulated subject area by studying its model. To perform spectral analysis of ocular fundus images, 21 color ranges were specified. However, after spectral analysis, zero values were obtained for 3 color ranges, so the number of color ranges was reduced to 18. The technological efficiency and possibility of glaucoma diagnosis by ASC-analysis of digitized parameters of fundus images of the eye in the intellectual system "Eidos" is shown. From the ACRIMA eye image database at the average similarity degree of 0.588, 90.7% of images of healthy eyes were recognized, and at the average similarity degree of 0.558, – 74.42% of images of eyes affected by glaucoma. The disadvantages of the ACRIMA ocular fundus image database are different image sizes, the presence of black backgrounds and different color shades, including black and white images, which reduces the reliability of glaucoma recognition. Addressing these shortcomings may be the goal of a new study to help improve the reliability of glaucoma recognition. The reliability of glaucoma recognition can also be improved by increasing the number of digitized eye image parameters, such as those obtained by optical coherence tomography. Processing of color eye images is computationally complex and requires a large amount of memory to store the digitized data, since eye fundus images consist of several hundreds of thousands of pixels. The Eidos intelligent system is capable of storing spectral analysis results in a memory of no more than 2 GB. Image size for spectral analysis by "Eidos" system should be not more than 800×600 pixels. Digitized parameters of the ocular fundus images can be provided by the authors free of charge to the readers of the journal at their request for further studies for the purpose of glaucoma diagnostics. The obstacle for practical application of new techniques in medical institutions for glaucoma diagnostics is the long duration of processing of eye images by known methods. If we use already digitized values of ocular fundus parameters, then spectral analysis of ocular fundus images will have to be performed only for new patients, which will shorten the duration of the glaucoma diagnosis process. There is no need to purchase a license to use the Eidos intelligent system, it can be downloaded from the Internet and used free of charge.

Conflict of Interest Statement

The authors declare that the study was conducted in the absence of any commercial or financial relationship that could be construed as a potential conflict of interest.

Acknowledgments

The authors are grateful to scientists Diaz-Pinto, Andres; Morales, Sandra; Naranjo, Valery; Köhler, Thomas; Mossi, Jose M.; Navea, Amparo for the possibility of using the image database for diagnosing glaucoma using the Eidos system.

REFERENCES

[1] M. J. Burton, J. Ramke, A. P Marques et al., "The Lancet Global Health Commission on Global Eye Health: Vision Beyond 2020," *The Lancet Global Health Commission*, vol. 9, no. 4, pp. e489-e551, 2021, https://doi.org/10.1016/S2214-109X(20)30488-5.

[2] T. Dada, S. Verma, M. Gagrani, Sh. Bhartiya, N. Chauhan, K. Satpute, and N. Sharma, "Ocular and Systemic Factors Associated with Glaucoma," *J Curr Glaucoma Pract.*, vol. 16, no. 3, pp. 179-191, 2022, https://doi.org/10.5005/jp-journals-10078-1383.

[3] I. V. Wagner, M.W. Stewart, and S. K. Dorairaj, "Updates on the Diagnosis and Management of Glaucoma," *Mayo Clin Proc Innov Qual Outcomes*, vol. 6, no. 6, pp. 618-635, 2022, https://doi.org/10.1016/j.mayocpiqo.2022.09.007.

[4] Y. C. Tham, X. Li, T. Y. Wong, H. A. Quigley, T. Aung, and C. Y. Cheng, "Global Prevalence of Glaucoma and Projections of Glaucoma Burden Through 2040: A Systematic Review and Meta-Analysis," *Ophthalmology*, vol. 121, no. 11, pp. 2081-2090, 2014, https://doi.org/10.1016/j.oph-tha.2014.05.013.

[5] K. Allison, D. Patel, and O. Alabi, "Epidemiology of Glaucoma: The Past, Present, and Predictions for the Future," *Cureus*, vol. 12, no. 11, 2020, https://doi.org/10.7759/cureus.11686.

[6] H. Meyer, and T. Sandell. "XEN® Gel Implant for Glaucoma; Prospective Cohort Study in a High-Volume Department," *Open Journal of Ophthalmology*, vol. 13, pp. 208-220, 2023, https://doi.org/10.4236/ojoph.2023.132018.

[7] Y. Wang, C. Xin, M. Li et al., "Macular Vessel Density Versus Ganglion Cell Complex Thickness for Detection of Early Primary Open-Angle Glaucoma," *BMC Ophthalmol*, vol. 20, no. 17, pp. 1-9, 2020, https://doi.org/10.1186/s12886-020-1304-x.

[8] T. Bah, R. Balde, M. Sovogui, F. Hann, and D. Nonga. "Compliance with Medical Treatment in Primary Open-Angle Glaucoma (POAG) at the Centre for the Application of the Diploma of Specialized Studies in Ophthalmology (CADES/O)," *Open Journal of Ophthalmology*, vol. 12, pp. 382-391, 2022, https://doi.org/10.4236/ojoph.2022.124035.

[9] K. Vonor, K. W. G. Keke, Y. Nagbé, Y. Tété, R. A. Kuaovi-Koko, K. D. Ayéna, M. Banla, and K. P. Balo, "Direct Cost of Primary Open Angle Glaucoma Management," *Open Journal of Ophthalmology*, vol. 12, pp. 352-361, 2022, https://doi.org/10.4236/ojoph.2022.124032.

[10] F. Rodríguez-Robles, R. Verdú-Monedero, R. Berenguer-Vidal, J. Morales-Sánchez, and I. Selles-Navarro, "Analysis of the Asymmetry between Both Eyes in Early Diagnosis of Glaucoma Combining Features Extracted from Retinal Images and OCTs into Classification Models," *Sensors (Basel, Switzerland)*, vol. 23, no. 10, 4737, 2023, https://doi.org/10.3390/s23104737.
[11] P. Ichhpujani, D. C. Lo, V. Cvintal, M. Waisbourd, A. Averbuch, B. E. Leiby, J. S. Myers, G. L. Spaeth, and L. J. Katz, "Flicker Defined Form, Standard Perimetry and Heidelberg Retinal Tomography: Structure-Function Relationships," *Can J Ophthalmol*, vol. 50, no. 4, 290-296, 2015, https://doi.org/10.1016/j.jcjo.2015.05.010.
[12] A. R. Ran, C. Y. Cheung, X. Wang, H. Chen, L. Luo, P. P. Chan et al., "Detection of Glaucomatous Optic Neuropathy with Spectral-Domain Optical Coherence Tomography: A Retrospective Training and Validation Deep-Learning Analysis," *The Lancet Digital Health*, vol. 1, no. 4, pp. e172-e182, 2019, https://doi.org/10.1016/S2589-7500(19)30085-8.
[13] A. I. M. Miguel, A.B. Silva, and L. F. Azevedo, "Diagnostic Performance of Optical Coherence Tomography Angiography in Glaucoma: A Systematic Review and Meta-Analysis," *British Journal of Ophthalmology*, vol. 103, pp. 1677-1684, 2019, https://doi.org/10.1136/bjophthalmol-2018-313461.
[14] F. S. Lopes, I. Matsubara, I. Almeida et al., "Structure-Function Relationships in Glaucoma using Enhanced Depth Imaging Optical Coherence Tomography-Derived Parameters: A Cross-Sectional Observational Study," *BMC Ophthalmol*, vol. 19, no. 52, 2019, https://doi.org/10.1186/s12886-019-1054-9.
[15] J. G. Fujimoto, C. Pitris, S. A. Boppart, and M. E. Brezinski, "Optical Coherence Tomography: An Emerging Technology for Biomedical Imaging and Optical Biopsy," *Neoplasia (New York, N.Y.),* vol. 2, no. 1-2, pp. 9-25, 2000, https://doi.org/10.1038/sj.neo.7900071.
[16] G. Coscas, F. Bandello, and A. Loewenstein, "Optical coherence tomography," *Optical Coherence Tomography*, pp. 1-134, 2014, https://doi.org/10.1159/isbn.978-3-318-02564-4.
[17] J. Jagodzinska, E. Sarzi, M. Cavalier, M. Seveno, V. Baecker, C. Hamel, M. Péquignot, and C. Delettre, "Optical Coherence Tomography: Imaging Mouse Retinal Ganglion Cells In Vivo," *J. Vis. Exp*., vol. 127, p. e55865, 2017, https://doi.org/10.3791/55865.
[18] X. Fan, H. Xu, R. Zhai *et al.*, "Peripapillary Vascular Reactivity in Primary Open-Angle Glaucoma with High Myopia by Using Optical Coherence Tomography Angiography," *Front Med (Lausanne)*, vol. 9, p. 850483, 2022, https://doi.org/10.3389/fmed.2022.850483.
[19] R. P. Tornow, R. Kolar, J. Odstrcilik *et al.*, "Imaging Video Plethysmography Shows Reduced Signal Amplitude in Glaucoma Patients in the Area of the Microvascular Tissue of the Optic Nerve Head," *Graefes Arch Clin Exp Ophthalmol*, vol. 259, pp. 483-494, 2021, https://doi.org/10.1007/s00417-020-04934-y.
[20] K. Omodaka, T. Kikawa, S. Kabakura *et al.*, "Clinical Characteristics Of Glaucoma Patients with Various Risk Factors," *BMC Ophthalmol*, vol. 22, p. 373, 2022, https://doi.org/10.1186/s12886-022-02587-5.
[21] S. Maheshwari, R. B. Pachori, and U. R. Acharya, "Automated Diagnosis of Glaucoma using Empirical Wavelet Transform and Correntropy Features Extracted from Fundus Images," *IEEE Journal of Biomedical and Health Informatics*, vol. 21, no. 3, pp. 803-813, 2017, https://doi.org/10.1109/JBHI.2016.2544961.
[22] Y. Mrad, Y. Elloumi, M. Akil, and M. H. Bedoui, "A Fast and Accurate Method for Glaucoma Screening from Smartphone-Captured Fundus Images," *Innovation and Research in BioMedical Engineering*, vol. 43, no. 4, pp. 279-289, 2022, https://doi.org/10.1016/j.irbm.2021.06.004.
[23] M. Esengönül, and A. Cunha, "Glaucoma Detection using Convolutional Neural Networks for Mobile Use," *Procedia Computer Science*, vol. 219, pp. 1153-1160, 2023, https://doi.org/10.1016/j.procs.2023.01.396.
[24] H. Mahdi, and N. El Abbadi, "Glaucoma Diagnosis Based on Retinal Fundus Image: A Review," *Iraqi Journal of Science* , vol. 63, no. 9, pp. 4022-4046, 2022, https://doi.org/10.24996/ijs.2022.63.9.32.
[25] M. J. M. Zedan, M. A. Zulkifley, A. A. Ibrahim, A. M. Moubark, N. Azwan, N. A. M. Kamari, and S. R. Abdani, "Automated Glaucoma Screening and Diagnosis Based on Retinal Fundus Images using Deep Learning Approaches: A Comprehensive Review," *Diagnostics*, vol. 13, no. 13, p. 2180, 2023, https://doi.org/10.3390/diagnostics13132180.
[26] S. Aumann, S. Donner, J. Fischer, and F. Müller, "Optical Coherence Tomography (OCT): Principle and Technical Realization" In: J. Bille (eds) *High Resolution Imaging in Microscopy and Ophthalmology*, 2019, https://doi.org/10.1007/978-3-030-16638-0_3.
[27] A. Geevarghese, G. Wollstein, H. Ishikawa, and J. S. Schuman, "Optical Coherence Tomography and Glaucoma," *Annu Rev Vis Sci.*, vol. 7, pp. 693-726, 2021, https://doi.org/10.1146/annurev-vision-100419-111350.
[28] G. Łabuz, A. Rayamajhi, K. Komar *et al.*, "Infrared- and White-Light Retinal Sensitivity In Glaucomatous Neuropathy," *Sci Rep*, vol. 12, p. 1961, 2022, https://doi.org/10.1038/s41598-022-05718-6.
[29] R. Nunez, A. Harris, O. Ibrahim, J. Keller, C. K. Wikle, E. Robinson, R. Zukerman, B. Siesky, A. Verticchio, L. Rowe, and G. Guidoboni, "Artificial Intelligence to Aid Glaucoma Diagnosis and Monitoring: State of the Art and New Directions," *Photonics*, vol. 9, no. 11, p. 810, 2022, https://doi.org/10.3390/photonics9110810.
[30] L. Zhang, L. Tang, M. Xia, and G. Cao, "The Application of Artificial Intelligence in Glaucoma Diagnosis and Prediction," *Front. Celldev. Biol*., vol. 11, p. 1173094, 2023, https://doi.org/10.3389/fcell.2023.1173094.
[31] K. H. Hung., Y. C. Kao, Y. H. Tang. et al, "Application of a Deep Learning System in Glaucoma Screening and Further Classification with Color Fundus Photographs: A Case Control Study," *BMC Ophthalmol*, vol. 22, p. 483, 2022, https://doi.org/10.1186/s12886-022-02730-2.

[32] R. Mahum, R. Rehman, O. D. Okon, A. Alabrah, T. Meraj, H. T. Rauf, "A Novel Hybrid Approach Based on Deep CNN to Detect Glaucoma using Fundus Imaging," *Electronics*, vol. 11, no. 1, p. 26, 2022, https://doi.org/10.3390/electronics11010026.
[33] O. Kovalyk, J. Morales-Sánchez, R. Verdú-Monedero, I. Sellés-Navarro, A. Palazón-Cabanes, and J.-L. Sancho-Gómez, "PAPILA: Dataset with fundus images and clinical data of both eyes of the same patient for glaucoma assessment," *Scientific Data*, vol. 9, no. 1, 2022, https://doi.org/10.1038/s41597-022-01388-1.
[34] A. Diaz-Pinto, S. Morales, V. Naranjo, T. Köhler, J. M. Mossi, and A. Navea, "CNNs for Automatic Glaucoma Assessment using Fundus Images: An Extensive Validation (Version 1)," CNNs for automatic glaucoma assessment using fundus images: an extensive validation. *Biomedical engineering online*, vol. 18, pp. 1-19, 2019, https://doi.org/10.6084/m9.figshare.7613135.v1.
[35] E. V. Lutsenko, D. K. Bandyk, and L. P. Troshin, "The Solution of Problems of Ampelography by using ASC-Analysis of Images of Leaves in their External Contours (Generalization, Abstraction, Classification and Identification)," *Scientific Journal of KubGAU*, vol. 112, no. 8, pp. 1-49, 2015, https://doi.org/10.13140/RG.2.2.22798.43849.
[36] L. Ogiela, "Cognitive informatics in image semantics description, identification and automatic pattern understanding," *Neurocomputing*, vol. 122, pp. 58-69, 2013, https://doi.org/10.1016/j.neucom.2013.06.001.
[37] E. V. Lutsenko, "Theoretical Foundations, Mathematical Model and Software Tools for Automated System-Cognitive Analysis" *July*, vol. 1, pp. 10-13140, 2020, https://doi.org/10.13140/RG.2.2.21918.15685.
[38] E. V. Lutsenko, "Automated System-Cognitive Analysis of the Dependence of Agrophysical Indicators of the Soil on its Processing, Fertilizers and the Phase of Wheat Vegetation," July, 2022, https://doi.org/10.13140/RG.2.2.34682.
[39] E. V. Lutsenko, "Scenario and Spectral Automated System-Cognitive Analysis," July, 2021, https://doi.org/10.13140/RG.2.2.22981.37608.
[40] E. V. Lutsenko, "ASC-Analysis and the Eidos System as a Method and Tools for Solving Problems," Nov. 2021, https://doi.org/10.13140/RG.2.2.29823.74407.
[41] E. V. Lutsenko, "Identification of Atypical Objects and Artifacts in the Source Data, Assignment to New Classes of Atypical Objects and Removal of Artifacts in Mathematical Models of Automated System-Cognitive Analysis," *Scientific Journal of KubGAU*, vol. 184, no. 10, pp. 1-50, 2022, https://doi.org/10.13140/RG.2.2.22198.98881.
[42] P. Ichhpujani, S. Thakur, and G. L. Spaeth, "Contrast Sensitivity and Glaucoma," *Journal of Glaucoma*, vol. 29, no. 1, pp. 71-75, 2020, doi: https://doi.org/10.1097/ijg.0000000000001379.
[43] M. Samadbeik, F. Fatehi, M. Braunstein, B. Barry, M. Saremian, F. Kalhor, and S. Edirippulige, "Education and Training on Electronic Medical Records (EMRs) for health care professionals and students: A Scoping Review," *International Journal of Medical Informatics*, vol. 142, p. 104238, 2020, https://doi.org/10.1016/j.ijmedinf.2020.104238.

BIOGRAPHY OF AUTHORS

Parul Ichhpujani, Professor at Glaucoma Services, Department of Ophthalmology, Govt. Medical College and Hospital, Chandigarh, India. Email: parul77@rediffmail.com, ORCiD: http://orcid.org/0000-0001-6256-4002.

Vladimir Ryabtsev, Doctor of Engineering Sciences, Professor Information Technologies, Cherkassy Branch of Private Higher Education Establishment European University, Cherkassy, Ukraine. Email: akimonoke2013@gmail.com. ORCiD: http://orcid.org/ 0000-0002-0592-2413.

Tetyana Utkina, Ph.D. in Computer Science, Associate Professor, Department of Robotics and Specialized Computer Systems, Cherkassy State Technological University, Cherkassy, Ukraine. Email: t.utkina@chdtu.edu.ua. ORCID: http://orcid.org/0000-0002-6614-4133.